Resonant optical patterns in sodium vapor in a magnetic field

Ziad H. Musslimani
Department of Mathematics, Technion–Israel Institute of Technology, 32 000 Haifa, Israel

Len M. Pismen
Department of Chemical Engineering and Minerva Center for Nonlinear Physics of Complex Systems, Technion–Israel Institute of Technology, Technion City, Haifa 32000, Israel

(Received 11 June 1998)

We study two-dimensional optical pattern formation in sodium vapor with a single-feedback mirror in a magnetic field. Complex transverse patterns sustained by resonant interactions arise under conditions when wave and static composite modes are excited simultaneously. [S1050-2947(99)05201-4]

PACS number(s): 42.65.−k

I. INTRODUCTION

Experiments in nonlinear optical feedback devices revealed a variety of transverse patterns including rolls, squares, hexagons, various flowerlike multipetal structures, and quasicrystalline patterns (see [1,2] for review). One of the most interesting feedback systems employs as the nonlinear medium sodium vapor in a buffer gas atmosphere irradiated by circularly polarized light [3]. Here, unlike a usual Kerr medium, transverse structures originate in polarization instabilities that are absent in the standard scalar model of D'Alessandro and Firth [4].

In alkali metal vapor the symmetry of the generated patterns depends crucially on the polarization of the input light. For linearly polarized input fields, roll and square patterns are formed, whereas the preferred patterns are hexagons for circular polarization. Moreover, unlike a Kerr medium where the hexagons observed are of a single type, alkali metals show transitions between both positive and negative hexagons for a given polarization ellipticity of the input beam [5,6].

Motivated by the experiments carried out by Grynberg *et al.* [7] and later by Ackemann and Lange [6], Scroggie and Firth [8] have studied theoretically the alkali metal vapor system *without* external magnetic field. Through a combination of linear and nonlinear analysis supported by numerical simulations, they were able to predict the formation of squares, rolls, rhomboids, and hexagons for suitably chosen parameters. Moreover, selection of quasicrystalline patterns in a single-feedback mirror device with rubidium atoms has been analytically predicted and numerically observed by Leduc *et al.* [9].

Simulation of two-dimensional optical pattern formation in sodium vapor with external magnetic field was carried out by Logvin *et al.* [10]. It was shown that hexagonal patterns can be unstable against spatial harmonics or subharmonics with hexagonal symmetry, which results in the formation of ultrahexagons or subhexagons. This instability is due to interaction with a secondary solution branch with a wave number nearly resonant to the harmonics of the primary hexagons. Amplitude equations were derived based on symmetry consideration, to explain the mechanism of the formation of the hexagons.

More recently, Logvin *et al.* [11] have demonstrated numerically the existence of a new kind of nonstationary hexagonal structure formed due to resonant interaction between wave (Hopf) and static (Turing) modes. This pattern has been named ''winking hexagons'' since the brightness of the individual constituents creating the hexagonal lattice oscillates with time (see Fig. 3 of Ref. [11]). The recently reported triadic Hopf-static patterns [12], visualized as drifting spots in a rhomboidal arrangement, apparently, also belong to a class of structures formed by the resonant interaction between Hopf and static modes.

The analysis of patterns sustained by resonant interactions under conditions when wave and static modes are excited simultaneously has been recently carried out in a more general context by Rubinstein and Pismen [13,14]. They showed that the excited patterns may be saturated by the action of quadratic (three-wave) interactions only, and may exhibit periodic amplitude modulation on a slow time scale. It is the aim of this paper to analyze conditions of wave-static resonance and resulting dynamic quasicrystalline patterns for the optical feedback system based on sodium vapor in magnetic field. The paper is organized as follows. After formulating the basic material equations in Sec. II, we reiterate in Sec. III the linear stability analysis of the model equations outlined in Refs. [15,11], emphasizing simultaneous bifurcation of wave and static composite modes. Weakly nonlinear analysis and derivation of amplitude equations will be given in Sec. IV, and the character of the emerging pattern will be inferred by mapping the physical parameters of the system on the parameters of the amplitude equation.

II. MATERIAL EQUATIONS

The experimental system used by Lange and his coworkers consisted of a cell of length l filled by sodium vapor acting as a nonlinear medium, and a single-feedback mirror separated by a distance d from the nonlinear material (see Fig. 1 of Ref. [15] for the experimental scheme). This system is subject to an external magnetic field B, and illuminated by a circularly polarized light beam with the amplitude E_0.

We shall use a thin optical medium approximation neglecting diffraction within the nonlinear material. Then the electric field of the light beam transmitted through the cell is

given by $E_t = E_0 e^{-ik_0 l\chi/2}$, where χ is the response function of the nonlinear material to the circularly polarized light field, and k_0 is the wave number of the incident light. Taking into account diffraction in free space, we can write an expression for the reflected light by formally integrating the paraxial wave equation to give

$$E_r = \sqrt{R} e^{-id\nabla^2/k_0} E_t . \tag{2.1}$$

Here R is the reflection coefficient of the mirror.

The main origin of nonlinearity of the medium is the population difference between sublevels of the sodium ground state with different spin orientation induced by optical pumping. Neglecting interference effects and diffraction in the medium, the optical pump rate is given by

$$P = \frac{\mu_e^2}{4\hbar^2 \Gamma_2 (\Delta^2 + 1)} (|E_0|^2 + |E_r|^2), \tag{2.2}$$

where μ_e is the electric dipole moment of the sodium vapor in its ground state, Γ_2 denotes the relaxation rate of the optical coherence, and Δ is the detuning between the incident field and the atomic transition, normalized to Γ_2 [16]. Using Eq. (2.1), we can rewrite Eq. (2.2) as

$$P = I\left[1 + R \left| \exp\left(-i \frac{d}{k_0} \nabla^2 \right) \exp(-ik_0 l\chi/2) \right|^2 \right]. \tag{2.3}$$

Here $I = [\mu_e^2/4\hbar^2 \Gamma_2 (\Delta^2 + 1)] |E_0|^2$ represents the pump rates of the circularly polarized incident plane wave.

The dynamics of the material variables is based on the semiclassical Liouville equation describing the time evolution of the sodium vapor spin density matrix ρ in the presence of electric and magnetic interactions,

$$i\hbar \frac{d\rho}{dt} = [H_0 + H_B + H_E, \rho], \tag{2.4}$$

where H_0 denotes the Hamiltonian of the atomic system without external fields, and H_B and H_E represent the interaction of the atoms with the static magnetic field B and the light field E, respectively. The components of the Bloch vector $\boldsymbol{m} = (u, v, w)$ are expressed through the density matrix ρ as $u = \rho_{12} + \rho_{21}, v = i(\rho_{12} - \rho_{21})$, and $w = \rho_{11} - \rho_{22}$. The first two components are related to the expectation values of the spin components and the third one to the population conversion. The spatiotemporal evolution of the Bloch vector $\boldsymbol{m}$ is given by [17]

$$\partial_t \boldsymbol{m} = -(\gamma - D\nabla^2 + P)\boldsymbol{m} + \boldsymbol{\Omega} \times \boldsymbol{m} + P\hat{\boldsymbol{e}}_z . \tag{2.5}$$

Here γ is the collision-induced relaxation coefficient of the Bloch vector, D is the diffusivity, and $\boldsymbol{\Omega} = (\Omega_x, 0, \Omega_z - \Delta P)$ is an effective Larmor frequency vector whose z component is modified by the light intensity dependent term ΔP. Physically, this term can be interpreted as a light shift effect on the ground state Zeeman sublevels. The pump rate P is given by Eq. (2.3), with response function χ defined as [see Eq. (A28) of Ref. [17]]

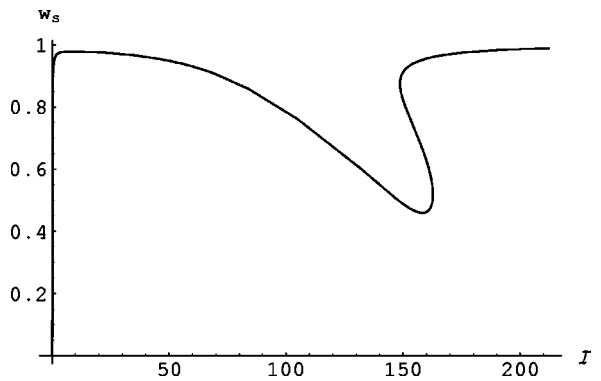

FIG. 1. Steady state orientation w_s versus pump intensity $\mathcal{I}$, for parameters $\Delta = -8.889$, $\Omega_z/2\pi = -264$ kHz, $\Omega_x/2\pi = 32$ kHz, $\gamma = 6$ Hz, $N = 10^{20}$ m^{-3}, $\Gamma_2/2\pi = 1.8$ GHz, and $\mu_e = 1.72 \times 10^{-29}$ C m. The dimensionless parameters are $\mathrm{Im}\kappa = -2.9$, $\theta_x/2\pi = 5.33 \times 10^3$, and $\theta_z/2\pi = 44 \times 10^3$.

$$\chi = -\frac{N\mu_e^2}{2\hbar\epsilon_0\Gamma_2} \frac{\Delta + i}{\Delta^2 + 1} (1 - w) \equiv \chi_0 (1 - w), \tag{2.6}$$

where N is the sodium particle density.

It is expedient to reformulate the problem in a dimensionless form. To this end, let us define the following parameters: $\kappa = k_0 l \chi_0, \delta^2 = D/\gamma, z = d/k_0, \boldsymbol{\theta} = \boldsymbol{\Omega}/\gamma, \mathcal{P} = P/\gamma,$ and $\mathcal{I} = I/\gamma$. We also set $R \approx 1$. After rescaling, Eqs. (2.5) and (2.3) take the following form:

$$\partial_t \boldsymbol{m} = [\delta^2 \nabla^2 - \mathcal{P}(\mathcal{I}, w) - 1]\boldsymbol{m} + \boldsymbol{\theta} \times \boldsymbol{m} + \mathcal{P}(\mathcal{I}, w)\hat{\boldsymbol{e}}_z , \tag{2.7}$$

$$\mathcal{P}(\mathcal{I}, w) = \mathcal{I}[1 + |\hat{\mathcal{D}}(z) e^{-i\kappa(1-w)/2}|^2], \tag{2.8}$$

where $\hat{\mathcal{D}}(z) = \exp(-iz\nabla^2)$ describes propagation and diffraction of the beam in the empty part of the cavity obtained by formal integration of the paraxial wave equation. Take note that $\hat{\mathcal{D}}(z) = \exp(izk^2)$ when it operates upon a pure mode with a transverse wave number k.

III. LINEAR ANALYSIS

The standard procedure of linear analysis involves testing stability to arbitrary infinitesimal perturbations, usually plane waves. Equations (2.7) and (2.8) admit a stationary homogeneous solution implicitly given by

$$[\mathcal{P}(\mathcal{I}, w_s) + 1]\boldsymbol{m}_s = \boldsymbol{\theta}(\mathcal{P}(\mathcal{I}, w_s)) \times \boldsymbol{m}_s + \mathcal{P}(\mathcal{I}, w_s)\hat{\boldsymbol{e}}_z . \tag{3.1}$$

A characteristic feature of the basic solution is a nonmonotonic dependence of the z component w_s of $\boldsymbol{m}_s$ on the external pump $\mathcal{I}$ [15] caused by the dependence of $\boldsymbol{\Omega}$ on the external pumping intensity that introduces a destabilizing positive feedback. This is shown in Fig. 1 where w_s is ploted against the external pump rate $\mathcal{I}$ [see Eq. (3) and Fig. 2(a) of Ref. [5]].

The next step in our analysis is to consider stability of the basic solution parametrized by w_s against superposition of plane waves. Proceeding in the standard way, we define $\boldsymbol{m}$

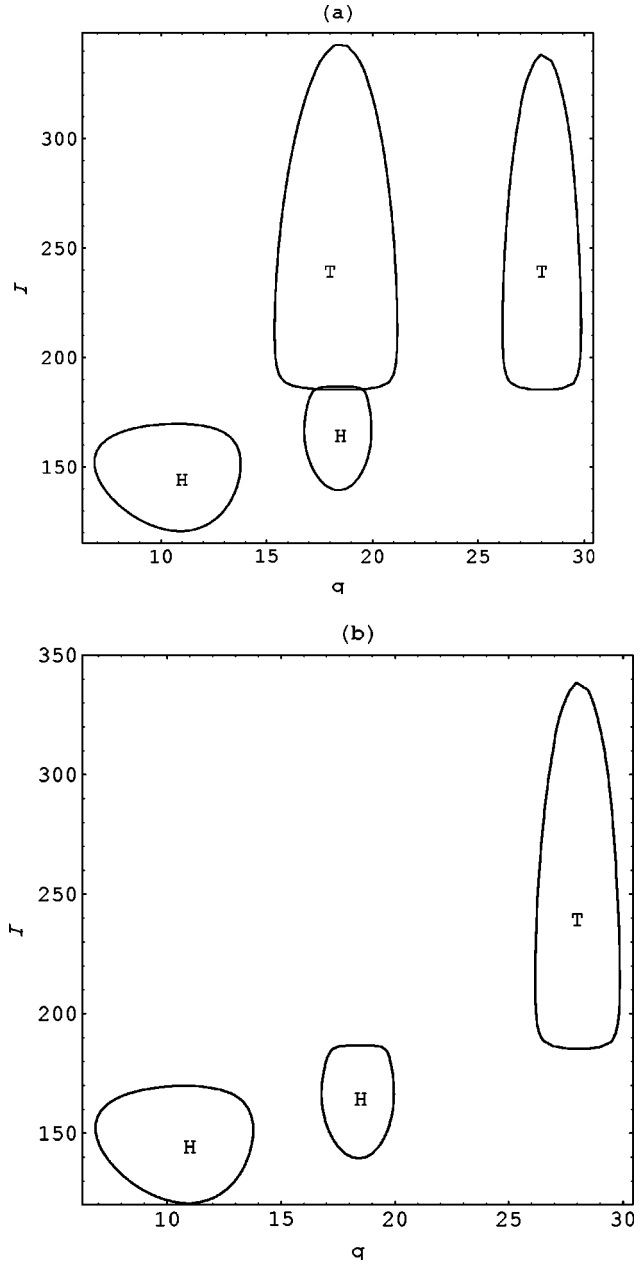

FIG. 2. Neutral stability curves in the $(\mathcal{I},q)$ space, corresponding to a wave mode (w) and a static mode (T) at $D=\delta=0$ (a) and $D=1$ cm^2/s, or $\delta=0.004$ (b). The values of other parameters are $k_0=2\pi/589.6$ nm^{-1}, $l=15$ mm, $\Delta=-8.889$, $R=0.915$, $\Omega_z/2\pi=-264$ kHz, $\Omega_x/2\pi=32$ kHz, $\gamma=6$ Hz, $d=150$ mm, $N=10^{20}$ m^{-3}, $\Gamma_2/2\pi=1.8$ GHz, and $\mu_e=1.72\times10^{-29}$ C m. The dimensionless parameters are $\mathrm{Im}\kappa=-2.9$, $\delta=0$, $\theta_x/2\pi=5.33\times10^3$, and $\theta_z/2\pi=44\times10^3$.

$=\boldsymbol{m}_s+\epsilon\boldsymbol{m}_1$ with $\epsilon\ll1$ and linearize system (2.7) and (2.8); we get the following eigenvalue problem:

$$\mathcal{L}\boldsymbol{m}_1\equiv[\partial_t-\delta^2\nabla^2+\mathcal{P}_s(\mathcal{I})+1]\boldsymbol{m}_1+\mathcal{I}\hat{\mathcal{T}}(z)W_1\boldsymbol{m}_s-\boldsymbol{\theta}_s\times\boldsymbol{m}_1+\hat{\boldsymbol{\theta}}_1(z)\times W_1\boldsymbol{m}_s-\mathcal{I}\hat{\mathcal{T}}(z)W_1\hat{\boldsymbol{e}}_z=\boldsymbol{0}. \tag{3.2}$$

Here $\boldsymbol{\theta}_s=\boldsymbol{\theta}(w_s)$, $\mathcal{P}_s(\mathcal{I})=\mathcal{P}(\mathcal{I},w_s)$, and W_1 is the z component of the Bloch vector deviation $\boldsymbol{m}_1$.

$$\hat{\mathcal{T}}(z)=e^{\mathrm{Im}\kappa(1-w_s)}[\mathrm{Re}\kappa\sin(z\nabla^2)-\mathrm{Im}\kappa\cos(z\nabla^2)], \tag{3.3}$$

and $\hat{\boldsymbol{\theta}}_1(z)=(0,0,\Delta\mathcal{I}\hat{\mathcal{T}}(z))$. Presenting the linear term $\boldsymbol{m}_1$ as the sum of $\mathcal{N}$ bifurcating modes with wave vectors $\boldsymbol{q}_i(i=1,2,\ldots,\mathcal{N})$,

$$\boldsymbol{m}_1=\sum_{j=1}^{\mathcal{N}}\boldsymbol{a}_j^{(1)}\exp(i\boldsymbol{q}_j\cdot\boldsymbol{x}+\sigma t)+\text{c.c.}, \tag{3.4}$$

and substituting into Eq. (3.2) we find that the basic solution loses stability on the marginal curve defined by [15]

$$\begin{vmatrix}\sigma+\mathcal{P}_{\mathrm{eff}} & \theta_z-\Delta\mathcal{P}_s & (u_s-\Delta v_s)\mathcal{T}\\ \Delta\mathcal{P}_s-\theta_z & \sigma+\mathcal{P}_{\mathrm{eff}} & (v_s+\Delta u_s)\mathcal{T}+\theta_x\\ 0 & -\theta_x & \sigma+\mathcal{P}_{\mathrm{eff}}-(1-w_s)\mathcal{T}\end{vmatrix}=0, \tag{3.5}$$

where $\mathcal{P}_{\mathrm{eff}}=1+\mathcal{P}_s(\mathcal{I})+\delta^2q^2$ and the spectrum of the operator $\hat{\mathcal{T}}(z)$ in the plane wave basis is given by

$$\mathcal{T}(zq^2)=-e^{\mathrm{Im}\kappa(1-w_s)}[\mathrm{Re}\kappa\sin(zq^2)+\mathrm{Im}\kappa\cos(zq^2)]. \tag{3.6}$$

Here $\boldsymbol{q}$ is the perturbation wave vector and σ is the corresponding eigenvalue. The curve $\mathrm{Re}\,\sigma(\mathcal{I},q)=0$ defines in the $(\mathcal{I},q)$ parameter space the marginal stability curve. If $\mathrm{Im}\,\sigma(\mathcal{I},q)$ vanishes at values of q where the real part of σ is minimal, then the instability is called static instability.

The neutral stability curves for static and Hopf instabilities, defined implicitly by Eq. (3.5), are plotted in Fig. 2 for zero and nonzero values of diffusivity and other parameters fitting the experimental conditions of Refs. [5,15]. For $\delta=0$ [Fig. 2(a)], there are additional instability zones located in the region of larger wave numbers which are not shown. With increasing diffusion, the instability domains shrink, and only one static instability zone is found at realistic values of diffusivity, as seen in Fig. 2(b).

Interaction between wave and static instabilities has formerly been detected in this system by Logvin *et al.* [11], who attributed to it the phenomenon of ''winking hexagons'' observed in their overlap range. Unlike the case studied in [11] where the instability regions overlapped in a wide range of pump intensities, we were able to find a set of parameters where the two instability thresholds are close to one another, so that the bifurcations are almost degenerate, as seen in Fig. 2. This allows us to treat the instabilities perturbatively, and to derive an amplitude equation governing the dynamics of slow amplitude modulation as in Refs. [13,14]. Moreover, in the absence of diffusion, we observe two static zones [Fig. 2(a)] in resonance with one wave mode, and the situation is close to a codimension 3 bifurcation.

IV. WEAKLY NONLINEAR ANALYSIS

Following a standard method of multiple scale bifurcation expansion, we introduce a hierarchy of time scales $t_0=t$, $t_1=\epsilon t$, . . . with

$$\partial/\partial t=\partial/\partial t_0+\epsilon\partial/\partial t_1+\epsilon^2\partial/\partial t_2+\cdots, \tag{4.1}$$

and expand in a power series the Bloch vector and the bifurcation parameter

$$\boldsymbol{m}=\boldsymbol{m}_s+\epsilon\boldsymbol{m}_1+\epsilon^2\boldsymbol{m}_2+\cdots, \tag{4.2}$$

$$\mathcal{I}=\mathcal{I}_0+\epsilon\mathcal{I}_1+\epsilon^2\mathcal{I}_2+\cdots. \tag{4.3}$$

Since the basic solution $\boldsymbol{m}_s$ depends on the bifurcation parameter via Eq. (3.1) we expand it in a power series

$$\boldsymbol{m}_s=\boldsymbol{m}_{s0}+\epsilon\boldsymbol{m}_{s1}+\epsilon^2\boldsymbol{m}_{s2}+\cdots.$$

Using the above expansions in system (2.7) and (2.8) we recover in the first order in ϵ the linear eigenvalue problem (3.2). In the next order we arrive at the following nonlinear inhomogeneous problem:

$$\begin{aligned}\mathcal{L}\boldsymbol{m}_2=&-\partial_{t_1}\boldsymbol{m}_1-[\mathcal{I}_0\hat{\mathcal{T}}(z)W_1+\mathcal{P}_s(\mathcal{I}_1)]\boldsymbol{m}_1-\mathcal{I}_0\hat{\mathcal{T}}(z)W_1\boldsymbol{m}_{s1}\\&+\hat{\mathcal{F}}(z)W_1\boldsymbol{m}_{s0}-\hat{\boldsymbol{\theta}}_1(z)\times W_1\boldsymbol{m}_{s1}-\hat{\boldsymbol{\theta}}_2(z)\times W_1\boldsymbol{m}_{s0}\\&-\hat{\boldsymbol{\theta}}_3(z)\times\boldsymbol{m}_1+\hat{\mathcal{F}}(z)W_1\hat{\boldsymbol{e}}_z,\end{aligned} \tag{4.4}$$

where $\mathcal{L}$ is defined in Eq. (3.2) and W_1 is the z component of $\boldsymbol{m}_1$. Here $\hat{\boldsymbol{\theta}}_2(z)W_1=(0,0,\Delta\hat{\mathcal{F}}(z)W_1)$ and $\hat{\boldsymbol{\theta}}_3(z)=\Delta(0,0,\mathcal{I}_0\hat{\mathcal{T}}(z)W_1+\mathcal{P}_s(\mathcal{I}_1))$. The operators $\hat{\mathcal{S}}(z)$ and $\hat{\mathcal{F}}(z)$ are defined by

$$\begin{aligned}\hat{\mathcal{S}}(z)=&\frac{1}{4}e^{\mathrm{Im}\kappa(1-w_{s0})}\{[(\mathrm{Im}\kappa)^2-(\mathrm{Re}\kappa)^2]\cos(z\nabla^2)\\&-2\mathrm{Re}\kappa\mathrm{Im}\kappa\sin(z\nabla^2)\},\end{aligned} \tag{4.5}$$

$$\begin{aligned}\hat{\mathcal{F}}(z)W_1=&(\mathcal{I}_1-\mathrm{Im}\kappa\mathcal{I}_0w_{s1})\hat{\mathcal{T}}(z)W_1+\mathcal{I}_0\hat{\mathcal{S}}(z)W_1^2\\&+\frac{1}{4}\mathcal{I}_0|\kappa|^2e^{\mathrm{Im}\kappa(1-w_{s0})}|\hat{\mathcal{D}}(z)W_1|^2.\end{aligned} \tag{4.6}$$

The amplitude equations are obtained as solvability conditions of Eq. (4.4), i.e., conditions of the orthogonality of the inhomogeneity to all eigenfunctions of the adjoint linear problem, with respect to the scalar product

$$\langle\boldsymbol{\phi}|\boldsymbol{\psi}\rangle=\sum_{j=1}^{3}\int\phi_j^*\psi_j d^2x.$$

A nontrivial solvability condition is obtained when the quadratic term (a product of two eigenfunctions, say ϕ_1 and ϕ_2) is in *resonance* with another eigenmode, say, ϕ_0. This requires that the frequencies and wave vectors of the three modes involved satisfy the resonance conditions

$$\boldsymbol{k}_1+\boldsymbol{k}_2=\boldsymbol{k}_0,\quad \omega_1+\omega_2=\omega_0. \tag{4.7}$$

A resonance triplet may involve therefore either three static modes or two wave modes from the same family (i.e., with identical frequencies) and one static mode.

A possible resonant structure consists of two wave modes with a given wave number k and one static mode with the wave number Q. This simplest resonant planform is expressed as

$$\boldsymbol{m}_1=a\boldsymbol{\alpha}_s e^{i\boldsymbol{Q}\cdot\boldsymbol{x}}+e^{i\omega t}\boldsymbol{\beta}_w(be^{i\boldsymbol{q}\cdot\boldsymbol{x}}+ce^{i\boldsymbol{k}\cdot\boldsymbol{x}})+\text{c.c.}, \tag{4.8}$$

where $\boldsymbol{\alpha}_s,\boldsymbol{\beta}_w$ are the eigenvectors of the linear problem corresponding to static and wave modes, respectively, and the resonance condition $\boldsymbol{q}-\boldsymbol{k}=\boldsymbol{Q}$ is satisfied. In order to derive dynamic equations for the amplitudes a, b, and c, one has to substitute Eq. (4.8) in the right hand side of Eq. (4.4), and then to project on the eigenfunctions of the adjoint problem. Keeping resonant terms only, we arrive after some algebra at the following system of amplitude equations which coincides with that obtained for optical cavities with rotated beam and two-component feedback optical system [13,14]:

$$\begin{aligned}\dot{a}&=\mu_s a+\nu_s bc^*,\\ \dot{b}&=\mu_w b+\nu_w ac,\\ \dot{c}&=\mu_w c+\nu_w a^*b.\end{aligned} \tag{4.9}$$

Here μ_s,μ_w depend on the deviation from the bifurcation point while ν_s,ν_w are computed at the bifurcation point; μ_s and ν_s are real, while μ_w and ν_w are complex. The expressions for the coefficients are given in the Appendix.

V. AMPLITUDE DYNAMICS

The three complex equations (4.9) can be reduced to four real equations for real amplitudes using the polar representation of the complex amplitudes,

$$a=\rho_a e^{i\theta_a},\quad b=\rho_b e^{i\theta_b},\quad c=\rho_c e^{i\theta_c}. \tag{5.1}$$

The relevant variables are the three real amplitudes ρ_j and the composite phase $\theta=\theta_a+\theta_c-\theta_b$. These equations can be further rescaled to a form containing two real parameters only. The imaginary part of μ_w can be absorbed in frequency, and three more real parameters are eliminated by rescaling the amplitudes and time. It can be shown that the condition $\mu_s<0$ is necessary to prevent runaway to large amplitudes (which may be further arrested by third and higher order terms). Assuming this condition holds, we rescale time by $|\mu_s|$ and denote $\mu=\mu_w/|\mu_s|$. The resulting equations are

$$\begin{aligned}\dot{\rho}_a&=-\rho_a+\rho_b\rho_c\cos\theta,\\ \dot{\rho}_b&=\mu\rho_b+\rho_a\rho_c\cos(\theta-\alpha),\\ \dot{\rho}_c&=\mu\rho_c+\rho_a\rho_b\cos(\theta+\alpha),\\ \dot{\theta}&=-\frac{\rho_b\rho_c}{\rho_a}\sin\theta-\frac{\rho_a\rho_b}{\rho_c}\sin(\theta+\alpha)-\frac{\rho_a\rho_c}{\rho_b}\sin(\theta-\alpha),\end{aligned} \tag{5.2}$$

where we have set $\nu_w=\nu e^{-i\alpha}$.

The bifurcation diagram of Eq. (5.2) has been constructed in Ref. [14]. At $\mu>0$, the trivial state is unstable and the dynamics saturates at small amplitudes. In different parametric domains, the system may relax to a stationary state, either symmetric ($\rho_b=\rho_c$) or asymmetric ($\rho_b\neq\rho_c$) with respect to the two wave modes, to a periodic orbit that corresponds to a slow modulation of the basic pattern on an extended time scale of Eq. (4.9), or to a chaotic attractor on the same extended scale.

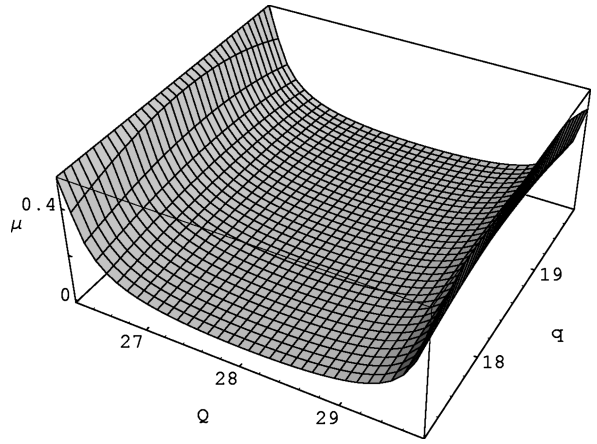

FIG. 3. Dependence of the parameter μ on Q and q, for model parameters used in Fig. 2(a).

Employing the expressions for the coefficients from the Appendix allows us to identify the dynamics corresponding to the actual parameters used in Fig. 2(b). Since only the *ratio* of the parameters dependent on the deviation from the bifurcation point is dynamically relevant, only a single point can be obtained (in the frame of Fig. 4) assuming an exact codimension 2 bifurcation with extrema of the wave and static neutral curves lying on the same level of pump intensity. One can see, however, that both extrema in Fig. 2(b) are rather flat, so that quite a long range of wave numbers falls into a narrow $O(\epsilon)$ interval of $\mathcal{I}$. Keeping in mind that the wave number may be constrained by geometry, we can choose any wave numbers falling in this range, provided they satisfy the resonance condition, and use the corresponding values in the formulas from the Appendix (see where the dependence of the parameter μ on Q and q is shown in Fig. 3). The parameter α is constant, since it is uniquely determined by the position of the bifurcation point. The range of possible regimes corresponding to a 1% variation of $\mathcal{I}$ is shown by the dashed vertical line in Fig. 4. This line crosses the domains of periodic and symmetric periodic solutions in the bifurcation diagram, and passes through the region of chaotic solutions in the vicinity of the separatrice shown by the dashed diagonal line in this figure. Such chaotic behavior was observed experimentally by Ackemann *et al.* in Fig. 4(b) of Ref. [5].

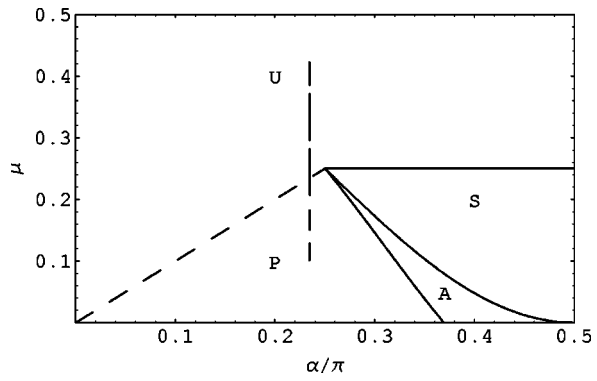

FIG. 4. Bifurcation diagram of Eq. (5.2) in the parametric plane (α,μ). Letters *S* and *A* denote the regions of stable stationary symmetric and asymmetric solutions; *P* stands for a pair of periodic solutions, and *U* for a symmetric periodic solution or other symmetric dynamic attractor. The dashed line shows an approximate location of the saddle-loop bifurcation. The dynamics corresponding to the actual parameters used in Fig. 2(b) is indicated by the dashed vertical line.

The variation of wave numbers within this range corresponds to the angle φ between the two wave modes in the resonant triangle varying from about 57° to 99°. For $\varphi=\pi/n$ where n is an integer, one can envisage a composite structure formed by $2n$ wave and n static modes that would usually correspond to a dynamical quasicrystalline pattern. Owing to the fact that no analogous structure was reported experimentally in a sodium vapor system in magnetic field, one might expect to see them in the future. These quasicrystals include perfect nonstationary hexagons with $\varphi=\pi/3$, in agreement with the recently reported ''winking hexagons'' obtained in Ref. [11], and dynamical square patterns (not yet found in experiments) with $\varphi=\pi/2$. Note that several kinds of patterns have been predicted by our bifurcation analysis. Particularly, the bifurcation diagram (Fig. 4) contains stationary hexagons (stationary *S* solutions) observed in experiments by Lange and co-workers in Refs. [5,15]. The dynamics, assuming the amplitudes of all static modes to be equal, and those of wave modes, pairwise equal, is defined by the same Eq. (4.9) or (5.2). In the case of hexagons, an additional term proportional to ρ_a^2 has to be included to account for the static-static resonant term. The selection of a pattern based on a single resonant triangle or their combination, as well as selection among propagating or standing wave modes, should be decided by relatively weak nonresonant quartic interactions.

ACKNOWLEDGMENTS

The authors are grateful to W. Lange, A. Nepomnyashchy, and B. Rubinstein for helpful discussions.

APPENDIX

The coefficients μ_s,μ_w,ν_s, and ν_w appearing in the amplitude equations (4.9) are given by

$$\mu_s=\mathcal{P}_{\rm eff}^2\xi_1+\mathcal{P}_{\rm eff}\theta_x\eta_1+(\theta_z-\Delta\mathcal{P}_s)^2\xi_1+\theta_x(\theta_z-\Delta\mathcal{P}_s)\zeta_1,$$

$$\nu_s=\mathcal{P}_{\rm eff}^2\xi_2+\mathcal{P}_{\rm eff}\theta_x\eta_2+(\theta_z-\Delta\mathcal{P}_s)^2\xi_2+\theta_x(\theta_z-\Delta\mathcal{P}_s)\zeta_2,$$

$$\mu_w=\mathcal{P}_{\rm eff}^2f_1+\mathcal{P}_{\rm eff}\theta_xg_1+(\theta_z-\Delta\mathcal{P}_s)^2f_1+\theta_x(\theta_z-\Delta\mathcal{P}_s)h_1,$$

$$\nu_w=\mathcal{P}_{\rm eff}^2f_2+\mathcal{P}_{\rm eff}\theta_xg_2+(\theta_z-\Delta\mathcal{P}_s)^2f_2+\theta_x(\theta_z-\Delta\mathcal{P}_s)h_2,$$

The functions $\xi_j,\eta_j,\zeta_j,f_j,g_j,h_j$ with $j=1$ depend on the deviation $\mathcal{I}_1$ from a degenerate bifurcation point, and those with $j=2$ are fixed. The explicit expressions are written below:

$$\xi_1=\mathcal{P}_s(\mathcal{I}_1)\alpha_{3s}+\alpha_{3s}[\mathcal{I}_0w_{s1}-(w_{s0}+1)\times(\mathcal{I}_1-{\rm Im}\kappa\mathcal{I}_0w_{s1})]\mathcal{T}(zQ^2),$$

$$\xi_2 = 2\mathcal{I}_0|\beta_{3w}|^2\mathcal{T}(zq^2) - 2\mathcal{I}_0|\beta_{3w}|^2(w_{s0}+1)\left[\mathcal{S}(zQ^2) + \frac{|\kappa|^2}{4}e^{\mathrm{Im}\kappa(1-w_{s0})}\right],$$

$$\eta_1 = \mathcal{P}_s(\mathcal{I}_1)(\alpha_{1s}+\Delta\alpha_{2s}) + \alpha_{3s}[\mathcal{I}_0 v_{s1} + \Delta\mathcal{I}_1 u_{s1} - (\mathcal{I}_1 - \mathrm{Im}\kappa\mathcal{I}_0 w_{s1})(v_{s0}-\Delta u_{s0})]\mathcal{T}(zQ^2),$$

$$\eta_2 = 2\mathrm{Re}[\beta_{3w}^*(\beta_{2w}+\Delta\beta_{1w})]\mathcal{I}_0\mathcal{T}(zq^2) - 2\mathcal{I}_0|\beta_{3w}|^2(v_{s0} - \Delta u_{s0})\left(\mathcal{S}(zQ^2) + \frac{|\kappa|^2}{4}e^{\mathrm{Im}\kappa(1-w_{s0})}\right),$$

$$\zeta_1 = \mathcal{P}_s(\mathcal{I}_1)(\alpha_{1s}-\Delta\alpha_{2s}) + \alpha_{3s}[\mathcal{I}_0 u_{s1} - \mathcal{I}_1\Delta v_{s1} - (\mathcal{I}_1 - \mathrm{Im}\kappa\mathcal{I}_0 w_{s1})(u_{s0}+\Delta v_{s0})]\mathcal{T}(zQ^2),$$

$$\zeta_2 = 2\mathrm{Re}[\beta_{3w}^*(\beta_{1w}-\Delta\beta_{2w})]\mathcal{I}_0\mathcal{T}(zq^2) - 2\mathcal{I}_0|\beta_{3w}|^2(u_{s0} + \Delta v_{s0})\left(\mathcal{S}(zQ^2) + \frac{|\kappa|^2}{4}e^{\mathrm{Im}\kappa(1-w_{s0})}\right),$$

$$f_1 = \beta_{3w}\mathcal{P}_s(\mathcal{I}_1) + \beta_{3w}[\mathcal{I}_0 w_{s1} - (w_{s0}+1) \times (\mathcal{I}_1 - \mathrm{Im}\kappa\mathcal{I}_0 w_{s1})]\mathcal{T}(zq^2),$$

$$f_2 = \mathcal{I}_0\alpha_{3s}\beta_{3w}[\mathcal{T}(zQ^2) + \mathcal{T}(zq^2)] - 2\mathcal{I}_0\alpha_{3s}\beta_{3w}(w_{s0}+1) \times\left(\mathcal{S}(zq^2) + \frac{|\kappa|^2}{4}e^{\mathrm{Im}\kappa(1-w_{s0})}\cos[z(Q^2-q^2)]\right),$$

$$g_1 = \mathcal{P}_s(\mathcal{I}_1)(\beta_{1w}+\Delta\beta_{2w}) + \beta_{3w}[\mathcal{I}_0 v_{s1} + \Delta\mathcal{I}_1 u_{s1} - (\mathcal{I}_1 - \mathrm{Im}\kappa\mathcal{I}_0 w_{s1})(v_{s0}-\Delta u_{s0})]\mathcal{T}(zq^2),$$

$$g_2 = \mathcal{I}_0\alpha_{3s}(\beta_{2w}+\Delta\beta_{1w})\mathcal{T}(zQ^2) + \mathcal{I}_0\beta_{3w}(\alpha_{2s} + \Delta\alpha_{1s})\mathcal{T}(zq^2) - 2\alpha_{3s}\beta_{3w}\mathcal{I}_0(v_{s0}-\Delta u_{s0})\left(\mathcal{S}(zq^2) + \frac{|\kappa|^2}{4}e^{\mathrm{Im}\kappa(1-w_{s0})}\cos[z(Q^2-q^2)]\right),$$

$$h_1 = \mathcal{P}_s(\mathcal{I}_1)(\beta_{1w}-\Delta\beta_{2w}) + \beta_{3w}[\mathcal{I}_0 u_{s1} - \Delta\mathcal{I}_1 v_{s1} - (\mathcal{I}_1 - \mathrm{Im}\kappa\mathcal{I}_0 w_{s1})(u_{s0}+\Delta v_{s0})]\mathcal{T}(zq^2),$$

$$h_2 = \mathcal{I}_0\alpha_{3s}(\beta_{1w}-\Delta\beta_{2w})\mathcal{T}(zQ^2) + \mathcal{I}_0\beta_{3w}(\alpha_{1s} - \Delta\alpha_{2s})\mathcal{T}(zq^2) - 2\alpha_{3s}\beta_{3w}\mathcal{I}_0(u_{s0}+\Delta v_{s0})\left(\mathcal{S}(zq^2) + \frac{|\kappa|^2}{4}e^{\mathrm{Im}\kappa(1-w_{s0})}\cos[z(Q^2-q^2)]\right).$$

Here $\mathcal{S}(zq^2)$ denotes the spectrum of the operator $\hat{\mathcal{S}}(z)$ in the plane wave basis.

[1] F. T. Arecchi, Physica D **86**, 297 (1995).
[2] L. A. Lugiato, M. Brambilla, and A. Gatti, Adv. At. Mol. Opt. Phys. (to be published).
[3] W. Lange, A. Aumann, T. Ackemann, and E. Buthe, Quantum Semiclassic. Opt. **10**, R23 (1998).
[4] G. D'Alessandro and W. J. Firth, Phys. Rev. Lett. **66**, 2597 (1991); Phys. Rev. A **46**, 537 (1992).
[5] T. Ackemann, Yu. A. Logvin, A. Heuer, and W. Lange, Phys. Rev. Lett. **75**, 3450 (1995).
[6] T. Ackemann and W. Lange, Phys. Rev. A **50**, R4468 (1994).
[7] G. Grynberg, A. Maitre, and A. Petrossian, Phys. Rev. Lett. **72**, 2379 (1994).
[8] A. J. Scroggie and W. J. Firth, Phys. Rev. A **53**, 2752 (1996).
[9] D. Leduc, M. Le Berre, E. Ressayre, and A. Tallet, Phys. Rev. A **53**, 1072 (1996).
[10] Yu. A. Logvin, T. Ackemann, and W. Lange, Phys. Rev. A **55**, 4538 (1997).
[11] Yu. A. Logvin, T. Ackemann, and W. Lange, Europhys. Lett. **38**, 583 (1997).
[12] Yu. A. Logvin, B. A. Samson, A. A. Afanas'ev, A. M. Samson, and N. A. Loiko, Phys. Rev. E **54**, R4548 (1996).
[13] B. Y. Rubinstein and L. M. Pismen, Phys. Rev. A **56**, 4264 (1997).
[14] B. Y. Rubinstein and L. M. Pismen, Opt. Commun. **145**, 159 (1998).
[15] W. Lange, Yu. A. Logvin, and T. Ackemann, Physica D **96**, 230 (1996).
[16] In our notation, $\Delta = \overline{\Delta}$ used in Refs. [10,11].
[17] F. Mitschke, R. Deserno, W. Lange, and J. Mlynek, Phys. Rev. A **33**, 3219 (1986).